LIQUID METAL SWIRLING FLOW
AFFECTED BY TRANSVERSE MAGNETIC FIELD

D. Krasnov[1], *Yu.B. Kolesnikov*[1], *I.A. Belyaev*[2],
Ya.I. Listratov[3], *O. Zikanov*[4]

[1] *Technische Universitat Ilmenau, Ilmenau, Germany*
[2] *Joint Institute for High Temperatures of RAS (JIHT RAS), Moscow, Russia*
[3] *Moscow Power Engineering Institute (MPEI), Moscow, Russia*
[4] *University of Michigan-Dearborn, USA*

In this work we study numerically liquid metal flow in a square duct under the influence of a transverse magnetic field applied in a spanwise direction (coplanar). The key interest of the present study is an attempt of passive control of flow regimes developed under magnetic field and thermal loads by applying specially shaped conditions, such as swirling, at the duct inlet. In this paper, we report results of numerical simulations of the interaction of swirling flow and transverse magnetic field in a square duct flow. Analysis of the obtained regimes might be important for the development of an experimental setup, in order to design corresponding inlet sections.

Introduction. Liquid metal flows under high thermal loads and strong transverse magnetic fields are of great interest for the development of cooling systems used in the present and future designs of fusion reactors [1]. Liquid metals are considered as very efficient coolants, since they can withstand significant heat loads and high temperatures without requiring high pressure in the system. Their use, however, may be constrained by a lack of understanding of magnetohydrodynamic (MHD) and thermogravitation convection (TGC) effects. So far, the accumulated theoretical and experimental knowledge [2–5] about convection processes under strong magnetic fields give us the following picture. The joint effect of electromagnetic and buoyancy forces on the liquid metal flow gives rise to instabilities leading to large-scale secondary vortices developing on the background of the main flow. As experiments show, there are ranges of parameters (in terms of the Hartmann, Reynolds, Grashof numbers), in which this phenomenon results in intermittent regimes characterized by high-amplitude, low-frequency fluctuations of temperature [6, 7], hot and cold spots, and unexpectedly high unsteady thermal loads at the walls. Obviously, from the engineering point of view, this behavior is undesirable, so that efforts are undertaken to eliminate the effect or to minimize its negative impact on heat and mass transfer.

This study is performed as a collaborative research project on thermal convection instabilities as well as on their dynamics and transformation under the magnetic field influence. The ultimate goal of the project, which involves both experimental and numerical studies, is passive control in order to minimize or at least to significantly affect the formation of thermal convection instabilities. The passive control can involve, for example, an inlet disturbance of prescribed form and shape. One of the potential candidates is the flow swirling which can be imposed at the duct inlet to set the fluid into rotating motion. It is known that in non-MHD flows swirling is preserved at large distances from the inlet [8]. Swirling generators can be relatively easily implemented in experiments, thus, proving a seemingly easy way for additional flow mixing expected even at low R_u. At the same time, the presence of a strong wall-normal magnetic field

may significantly alter this process due to the suppression velocity fluctuations and anisotropy introduced by the magnetic field. Therefore, the interaction of flow swirling with a transverse magnetic field poses a non-trivial stand-alone problem, which has not been addressed so far. At the present stage of our study, we consider this problem in the cleanest possible settings of isothermal fluid and in the square duct geometry.

1. Problem formulation.

1.1. Physical model and equations. We consider an isothermal flow of an incompressible electrically conducting fluid, e.g., liquid metal, in a square duct of half-height a and length L_x. The flow is driven by a pressure gradient $\partial P_0/\partial x$ in the streamwise x-direction. A transverse magnetic field $\mathbf{B}$ is imposed along the spanwise y-direction.

In the assumption of small magnetic Reynolds and Prandtl numbers, the quasi-static approximation [9, 10] of the MHD interactions is applied. The non-dimensional governing equations become

$$\frac{\partial \mathbf{u}}{\partial t} + (\mathbf{u} \cdot \nabla)\mathbf{u} = -\nabla p + \frac{1}{\mathrm{Re}} \cdot \nabla^2 \mathbf{u} + \mathrm{N}(\mathbf{j} \times \mathbf{e}_b), \tag{1}$$

$$\nabla \cdot \mathbf{u} = 0. \tag{2}$$

Here $\mathbf{u}$, p and $\mathbf{j}$ are the fields of velocity, pressure and the electric current density, whereas $\mathbf{e}_b$ is the non-dimensional imposed magnetic field. The electric current $\mathbf{j}$ is determined by the Ohm's law

$$j = -\nabla\phi + \mathbf{u} \times \mathbf{e}_b, \tag{3}$$

where the electric potential ϕ is a solution of the Poisson equation expressing the electric neutrality of the liquid

$$\nabla^2 \phi = \nabla \cdot (\mathbf{u} \times \mathbf{e}_b). \tag{4}$$

Eqs. (1)–(4) are non-dimensionalized using the mean streamwise velocity U, the duct half-height a and the magnetic field B maximum as characteristic scales of velocity, length and magnetic field, respectively. The non-dimensional parameters of the problem are the Reynolds number

$$\mathrm{Re} \equiv \frac{aU}{\nu}, \tag{5}$$

and the Hartmann number

$$\mathrm{Ha} \equiv aB\sqrt{\frac{\sigma}{\rho\nu}}, \tag{6}$$

or the magnetic interaction parameter (the Stuart number)

$$\mathrm{St} \equiv \frac{\mathrm{Ha}^2}{\mathrm{Re}} \equiv \frac{\sigma a B^2}{\rho U}. \tag{7}$$

1.2. Boundary conditions. The boundary conditions at the duct walls include the non-slip condition for the velocity field and the condition of perfect electric insulation

$$\mathbf{u} = 0 \quad \text{and} \quad \frac{\partial \phi}{\partial n} = 0 \quad \text{at} \quad y, z = \pm a. \tag{8}$$

The boundary condition $\partial \phi/\partial x = 0$ is prescribed at the inlet and outlet sections. This allows the electric currents j to enter and exit the duct thus assuming a virtual closure of the loops outside the domain. For the velocity at the inlet, we supply a basic

profile with all three velocity components prescribed. The profile may present different flow regimes, such as a laminar duct flow, a honeycomb pattern, a profile with swirl, etc. The simulations presented below are for the inlet conditions in the form of laminar parabolic without or with imposed swirl (see a detailed discussion below). The convective condition is imposed at the outlet:

$$\partial \mathbf{u}/\partial t + U \partial \mathbf{u}/\partial x = 0, \tag{9}$$

where U is the mean flux velocity. At each time step, both the inlet and outlet velocity fields are normalized so that their mean velocity U is exactly unity, which allows us to avoid numerical instability and achieve fast convergence with the target flow regimes.

2. Numerical method.

2.1. Scheme. The system of governing equations (1)–(4) is solved numerically with our in-house DNS solver for rectangular geometries. It is based on the second-order finite-difference method with collocated grid arrangement, following the conservation principles for mass, momentum and kinetic energy developed in [11] and later extended to MHD flows in [12]. Time discretization is based on the fully explicit Adams–Bashforth/Backward–Differentiation method of second order [13]. The incompressibility condition for velocity $\mathbf{u}$ is satisfied by applying a standard projection method [14]. Every time step requires solution of elliptic problems for pressure and electric potential. The in- and outflow conditions are tackled by applying cosine series expansions in the streamwise x-direction, so that the fully 3D elliptic problems are transformed into a series of much simpler 2D problems. The code is parallelized with a hybrid approach, using both MPI and OpenMP libraries. More details on the solver and its verification can be found in our prior studies, e.g., in [15–17].

2.2. Grid size. The simulations have been performed in a square duct geometry with the domain size $L_x \times L_y \times L_z = 8\pi \times 2 \times 2$ and numerical resolution $n_x \times n_y \times n_z = 2048 \times 128 \times 128$ points, correspondingly, in the streamwise x- and two wall-normal (transverse) y, z-directions. In the streamwise direction, the grid was uniform, whereas in the wall-normal directions we have used a grid with clustering towards the walls to resolve thin boundary layers, especially at high Ha numbers. For the y, z grid clustering, a modified Gauss–Lobatto stretching was applied

$$z = g(\eta) = \sin\left(0.5\pi \sinh\left(\eta\right)/\sinh\left(1\right)\right). \tag{10}$$

Here z is the real non-uniform coordinate and η is the transformed uniform coordinate, both varying within $[-1 \dots 1]$. The advantage of using stretching (Eq. 10) versus classic Gauss–Lobatto $z = \sin\left(0.5\pi\eta\right)$ is that it provides smaller cell sizes (i.e. better resolution) in the core region while retaining a comparably strong clustering at the walls. Finally, to avoid extremely small cell sizes at the walls, we have used a linear blending between the non-uniform (Eq. 10) and uniform coordinates: $z = 0.9g(\eta) + 0.1\eta$, which also assists in maintaining reasonably large integration time-steps Δt at high resolutions.

3. Results.
The simulations have been performed for several Reynolds numbers (Re $= 500$, 1500 and 3000), several Hartmann numbers (Ha $= 0 \dots 100$) and two magnitudes of the inlet swirling. The swirling was specified using an equation for the Burger's vortex (see Fig. 1a). The equation defines the azimuthal velocity component u_ϕ versus radius and allows modifying the radial distribution, position of the maximum and the magnitude. The swirling magnitudes were specified as ratios between the maximum
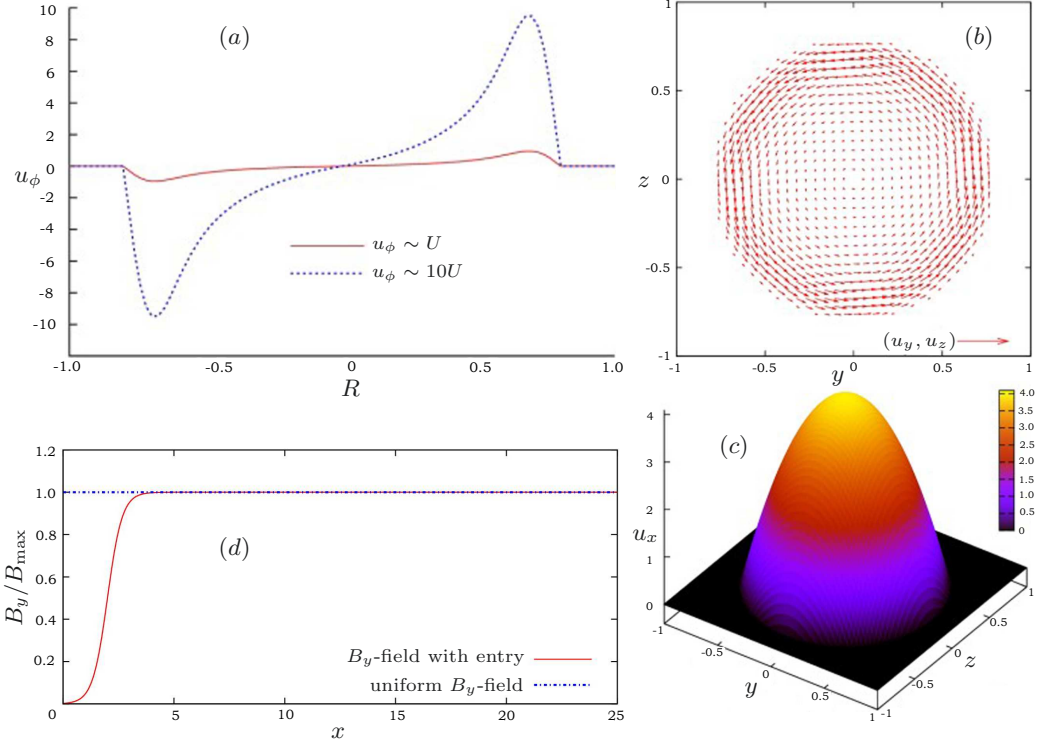
D. Krasnov, Yu.B. Kolesnikov, I.A. Belyaev, Ya.I. Listratov, O. Zikanov

Fig. 1. Illustration of the inlet velocity distribution. (*a*) The distribution of the azimuthal velocity u_ϕ vs. radius R is shown for two amplitudes $u_\phi = U$ and $u_\phi = 10U$, where U is the mean streamwise velocity. The swirling is specified in the circle $R \leq 0.8$. The velocity components u_y and u_z at the inlet section of the duct are shown in the plot (*b*). The streamwise velocity as a circular parabolic profile is shown in the plot (*c*). (*d*) The distribution of the main component B_y of the magnetic field is shown.

value of the azimuthal velocity at the inlet and the mean streamwise velocity U: moderate swirling with $u_\phi = U$ and strong swirling with $u_\phi = 10U$. The streamwise velocity at the inlet was prescribed in the form of an axisymmetric parabolic profile (see Fig. 1*c*) occupying 80% of the duct size. Note that the classical duct flow profile can be used there as well but gives this possibility to future studies. Also, to address the possible effects of entrering the magnetic field, we have considered two configurations: a completely uniform field and a non-uniform curl- and divergence-free magnetic field, approximated by [18], with a realistic entry region at about $x = 4$. The non-uniform field [18] had two components: the main one B_y (shown in Fig. 1) and B_x – a much weaker component which might, however, be significant around the inlet.

As the first result, we should mention that the swirling changed the flow pattern and significantly enhances stirring. Without swirling, the flow at such a moderate Reynolds number remains laminar and steady in the entire duct. This was observed both for Re below the typical laminar-turbulent transition range (about 2000) and for higher Re = 3000 when the duct length was insufficient for the development of a transition without swirling. The streamwise velocity profile was gradually flattened by the viscosity as the flow progressed downstream. The swirling rendered the flow pattern unsteady and much more complicated spatially, as illustrated in Figs. 2–5 and discussed in detail below.

The simulations indicated that, upon increasing Ha, the transverse magnetic field gradually suppressed the effect of swirling, making it less and less pronounced, as it moved the flow downstream. This can be observed by comparing the flow in Figs. 2 and 3 for, respectively, the non-MHD case and for Ha = 50 under the non-uniform field. The results for the non-MHD case have confirmed our earlier conclusion that the inlet swirling significantly enhances the overall flow mixing even at low Re, as seen, e.g., for the two sub-critical values Re = 500 and 1500. The flow is unsteady, fluctuating, and at Re = 1500 and 3000 apparently turbulent. The velocity profile turns around the duct's central axis due to the rotation introduced by the swirling.

The situation changed quite noticeably in the presence of the magnetic field. Albeit the flow mixing is still enhanced compared to a flow without swirling, the fluctuating flow structures become weaker due to the suppression by the magnetic field. Already at Ha = 50 (Fig. 3) the magnetic field appears to eliminate the effects produced by the
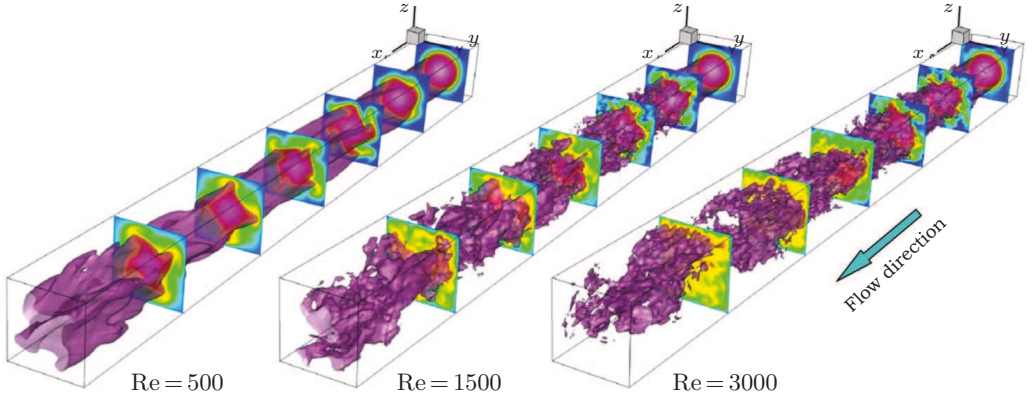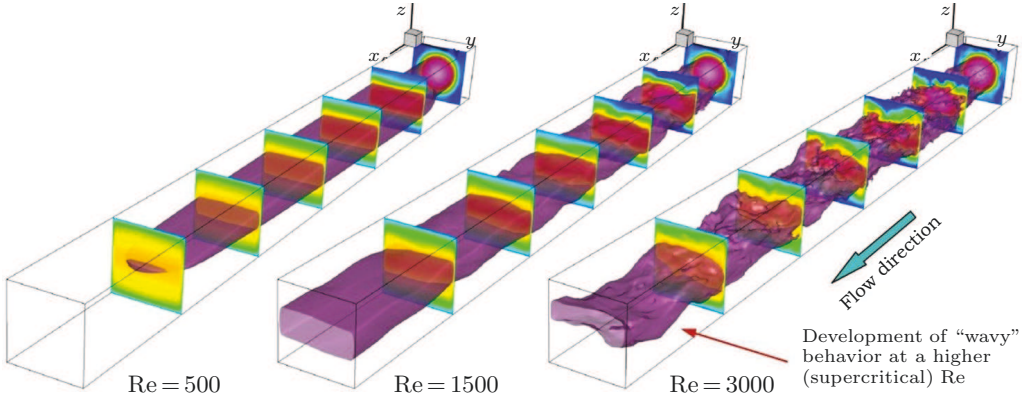

Fig. 2. Instantaneous snapshots of flow fields after 40 convective time units of evolution for the inlet swirling with the magnitude $u_\phi = U$ (moderate swirling) and Ha = 0 (non-MHD case). Shown are the isosurface of the streamwise velocity u_x (violet, level of $1.2U$) and several distributions of u_x in (y, z)-slices along the duct length.

Fig. 3. Instantaneous snapshots of flow fields after 40 convective time units of evolution for the inlet swirling with magnitude $u_\phi = U$ (moderate swirling) and Ha = 50 (magnetic field with inlet). Shown are the isosurface of the streamwise velocity u_x (violet, level of $1.2U$) and several distributions of u_x in (y, z)-slices along the duct length.
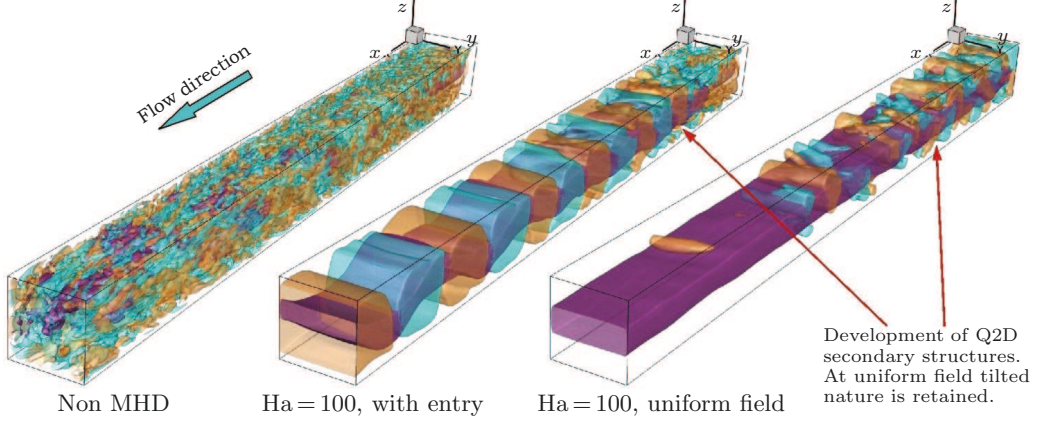
Fig. 4. Interaction of swirling flow and magnetic field illustrated by the DNS results at Re = 3000 and moderate swirling $u_\phi = U$. Instantaneous snapshots after 40 convective time units of evolution are shown for non-MHD case (left) and for non-uniform (middle) and uniform (right) configurations of the magnetic field at Ha = 100. Visualized are the streamwise velocity u_x (1.2U, violet) and secondary structures by the vertical velocity u_z ($\pm 0.05U$, cyan & brown).
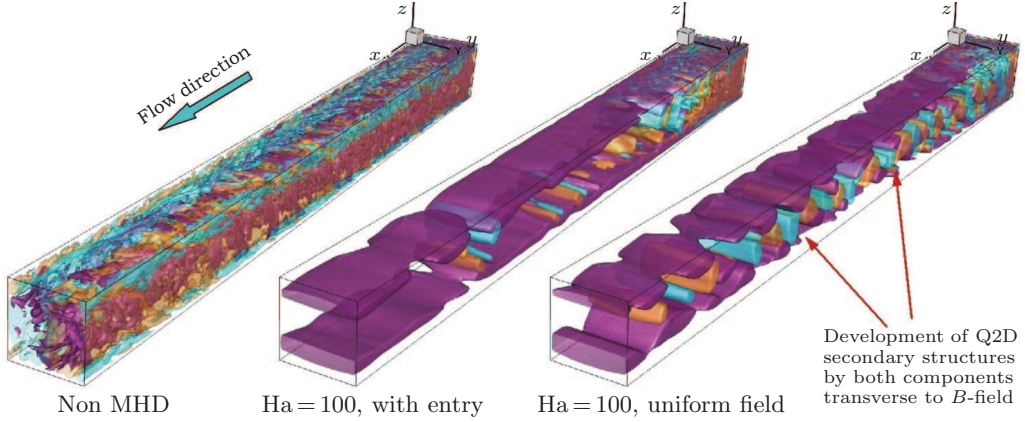

Fig. 5. Interaction of swirling flow and magnetic field illustrated by the DNS results at Re = 3000 and strong swirling $u_\phi = 10U$. Instantaneous snapshots after 40 convective units of spatio-temporal evolution are shown for non-MHD case (left) and for non-uniform (middle) a nd uniform (right) configurations of the magnetic field at Ha = 100. Visualized are the streamwise velocity (1.2U, violet) and secondary structures by the vertical velocity u_z ($\pm 0.05U$, cyan & brown).

imposed swirling, especially well observed at low Re. Another important effect is the influence of the magnetic field non-uniformity. The flow exhibits a transformation into a flat jet after passing through the inlet region. At higher Re, a wavy behavior appeared, which can be attributed to the residual fluctuations from the swirling.

At a certain value of Ha, further suppression of the residual structures ceased and, instead, the flow attained a quasi-2D form, which is illustrated in Figs. 4 and 5 for Re = 3000 and Ha = 100 and for magnitudes of the inlet swirling. One can see clearly

pronounced quasi-2D patterns (Fig. 4) as a result of the moderate swirling transformation under strong MHD effects. The effect of the magnetic field configuration is also visible: the inlet region has almost completely destroyed the swirling and produces large-scale quasi-2D vortices, whereas the uniform field tends to retain tilted rolls further, as seen in Fig. 4. When the swirling magnitude was further increased by a factor of 10, as shown in Fig. 5, the results immediately became somewhat counter-intuitive: contrary to the expectations, the stronger swirling did not enhance the mixing but, instead, resulted in a faster transformation towards a quasi-2D state. An enhanced two-dimensionality also appeared when planar sheets developed in the Shercliff layers. In this particular case, the effect of the field uniformity was much more pronounced. We observed a "pinch-like" instability of the planar sheets, whereas the secondary structures populated the entire bulk region up to the duct exit. It can be concluded that the interaction of a strong swirling with a strong uniform magnetic field rapidly introduces two-dimensionality into the flow. Note also that this result is consistent with a previous prior study of MHD flow past the honeycomb [19].

A possible explanation of this rather unexpected behavior under the uniform field can be suggested by analyzing the rotational components of the swirling flow, in particular, their interaction with the magnetic field. At the top and bottom walls (in the Shercliff layers), the rotational flow is represented by the spanwise velocity component u_y which is parallel to the magnetic field. At the side walls (in the Hartmann layers), the rotational flow is in the vertical component u_z, perpendicular to the field and experiencing the strong MHD braking effect. Obviously, the braking effect is proportional to the magnitude of the swirling and to the strength of the applied field. Moreover, because of incompressibility, the other two velocity components are also suppressed in the Hartmann layers. The flow develops an M-shaped profile of the streamwise velocity (see Fig. 5). Albeit the mechanism is different, the result of the braking is similar to the Hunt's flow. The planar jets in such profiles are susceptible to the Kelvin–Helmholtz instability, often observed at already low Re [20], which appears in the form of jet detachments. One can see that similar detachments also appeared in the considered case of strong swirling at the top and bottom walls (Fig. 5).

The numerical simulations have shown that the initial flow disturbance in the form of swirling does not retain the initial shape under a strong transverse magnetic field. Albeit under weak magnetic fields the flow mixing is still enhanced by the swirling, at stronger fields quasi-2D structures (vortices and rolls) form rapidly. Moreover, increasing the swirling magnitude does not prevent the flow from developing quasi-2D states. Instead, the two-dimensionality evolves even more rapidly, which was especially well observed in the case of the uniform magnetic field, where quasi-2D planar sheets and rolls fill the entire domain. This raises a question: how do the observed quasi-2D structures interfere with thermal convection effects? This question will be the subject of our next investigations.

Conclusions and outlook. We summarize the most important outcomes obtained in this study and present a plan of the next steps of our joint research.

- Numerical experiments have been performed for the duct flow exposed to the spanwise magnetic field in the range of $0 < \text{Ha} < 100$, $500 < \text{Re} < 3000$ with swirling applied at the inlet.

- The shape of the magnetic field in the inlet region has a strong effect on the process of initial flow transformation caused by swirling. This can be attributed not only to

the gradient of the main component B_y, but also to the secondary component B_x getting significant at the inlet.

- The more intense the swirling, the faster it transforms into quasi-2D structures, especially when the magnetic field is uniform along the channel. This causes a counter-intuitive result. A weaker swirling persists longer in the magnetic field than a swirling with a higher amplitude.

- A physically plausible explanation of this phenomenon, associated with the formation of M-shaped profiles and thin 2D sheets in the Shercliff layers under the uniform field and strong swirling, has been proposed.

Exact experimental validation of the observed phenomena at high values of swirling appears extremely complicated, since it needs special equipment to create such flow condition. However, numerical solutions can provide an insight into the underlying physics and principal behavior of the MHD swirling flow. Therefore, more detailed numerical assessment of the observed phenomena, including analysis of electric currents, time signals spectra and velocity correlations in the (y, z)-cross-sections is planned.

Based on the presented results, we formulate a feasible parameter range to deploy the experimental program and extend our numerical study by including heat transport, thus, making it as close as possible to the experimental conditions. Ultimately, we will target the experimental geometry of the duct with the aspect ratio $L_y/L_z = 3.5/1$, which will also allow us to introduce more than one swirling generator and address the effects of both co- and counter-rotating swirling flows under magnetic fields and thermal loads.

References

[1] I.R. KIRILLOV, C.B. REED, L. BARLEON, AND K. MIYAZAKI. Present understanding of MHD and heat transfer phenomena for liquid metal blankets. *Fusion engineering and design*, vol. 27 (1995), pp. 553–569.

[2] I. BELYAEV, *et al.* Features of MHD heat transfer in simple channels. *Magnetohydrodynamics*, vol. 54 (2018), no. 3, pp. 245–259; DOI: http://doi.org/10.22364/mhd.54.3.5

[3] I. KIRILLOV, *et al.* Buoyancy effects in vertical rectangular duct with coplanar magnetic field and single sided heat load–downward and upward flow. *Fusion Engineering and Design*, vol. 127 (2018), pp. 226–233.

[4] S. SMOLENTSEV, N. VETCHA, AND M. ABDOU. Effect of a magnetic field on stability and transitions in liquid breeder flows in a blanket. *Fusion Engineering and Design*, vol. 88 (2013), no. 6-8, pp. 607–610.

[5] L. LIU AND O. ZIKANOV. Elevator mode convection in flows with strong magnetic fields. *Physics of Fluids*, vol. 27 (2015), no. 4, p. 044103.

[6] N. Razuvanov, P. Frick, I. Belyaev, and V. Sviridov. Experimental study of liquid metal heat transfer in a vertical duct affected by coplanar magnetic field: Downward flow. *International Journal of Heat and Mass Transfer*, vol. 143 (2019), p. 118529.

[7] I. Belyaev, *et al.* Temperature fluctuations accompanying MHD heat transfer of liquid metal downflow in a pipe. *Fluid Dynamics Research*, vol. 50 (2018), no. 5, p. 051403.

[8] O. Kitoh. Experimental study of turbulent swirling flow in a straight pipe. *Journal of Fluid Mechanics*, vol. 225 (1991), pp. 445–479.

[9] P.A. Davidson. *Introduction to magnetohydrodynamics* (Cambridge University Press, 2016).

[10] P.H. Roberts. *An introduction to Magnetohydrodynamics* (Longmans, Green, New York, 1967).

[11] Y. Morinishi, T.S. Lund, O.V. Vasilyev, and P. Moin. Fully conservative higher order finite difference schemes for incompressible flow. *J. Comp. Phys.*, vol. 143 (1998), pp. 90–124.

[12] M.-J. Ni, *et al.* A current density conservative scheme for incompressible MHD flows at a low magnetic Reynolds number. Part I: On a rectangular collocated grid system. *J. Comp. Phys.*, vol. 227 (2007), pp. 174–204.

[13] R. Peyret. *Spectral Methods for Incompressible Viscous Flows* (Springer, New York, 2002).

[14] O. Zikanov. *Essential Computational Fluid Dynamics, 2nd Ed.* (Wiley, 2019).

[15] D. Krasnov, O. Zikanov, and T. Boeck. Comparative study of finite difference approaches to simulation of magnetohydrodynamic turbulence at low magnetic Reynolds number. *Comp. Fluids*, vol. 50 (2011), pp. 46–59.

[16] D.S. Krasnov, O. Zikanov, and T. Boeck. Numerical study of magnetohydrodynamic duct flow at high Reynolds and Hartmann numbers. *J. Fluid Mech.*, vol. 704 (2012), pp. 421–446.

[17] O. Zikanov, *et al.* Patterned turbulence in spatially evolving magnetohydrodynamic duct and pipe flows. *Theor. Comp. Fluid Dyn.*, vol. 28 (2014), pp. 319–334.

[18] E.V. Votyakov, S.C. Kassinos, and X. Albets-Chico. Analytic models of heterogenous magnetic fields for liquid metal flow simulations. *Theoretical and Computational Fluid Dynamics*, vol. 23 (2009), no. 6, pp. 571–578.

[19] O. Zikanov, D. Krasnov, T. Boeck, and S. Sukoriansky. Decay of turbulence in a liquid metal duct flow with transverse magnetic field. *J. Fluid Mech.*, vol. 867 (2019), pp. 661–690.

[20] L. Braiden, *et al.* Transition to turbulence in hunt's flow in a moderate magnetic field. *Europhysics Letters*, vol. 115 (2016), p. 44002.